7.6 Predictability and Sensitivity of Downslope Windstorms in San Diego County

Yang Cao and Robert G. Fovell*

Department of Atmospheric and Oceanic Sciences, University of California, Los Angeles

ABSTRACT

A case study of downslope flow during a moderately intense Southern California weather event known as the Santa Ana winds is presented, making use of an exceptionally dense network of near-surface observations in San Diego county to calibrate and validate a numerical weather prediction model, which in turn is used to help understand and fill in the many gaps in the observations. This case is shown to be particularly sensitive to the physical parameterizations and landuse database employed in the model, as well as to small random perturbations mimicking the action of unresolved turbulence.

1. Introduction

Southern California is famous for its "Santa Ana" winds, which were named after a city and canyon in Orange County. Santa Anas are very dry, sometimes hot, offshore winds (Glickman 2000) that can produce gusts exceeding 25 m s^{-1} (56 mph) in favored areas (Chow et al. 2012). Events occur most frequently between October and February, with December being the peak month, although its season extends from September through April (Raphael 2003). Although Santa Anas tend to form most frequently in midwinter, the most dangerous events often occur in autumn, before the winter rains have begun. At that time, the vegetation tends to be extremely dry, and autumn fires historically have the potential to be very large in area, being fanned by the Santa Ana winds (Chang and Schoenberg 2011).

Santa Ana events result when cooler air spills across the Great Basin, becoming partially dammed by the mountains that encircle Southern California. This increases the horizontal gradient in sea-level pressure (SLP) and helps increase flow speeds through prominent terrain gaps such as the Cajon Pass (leading to Santa Ana) and through the Soledad Gap (northwest of Los Angeles), creating prominent wind corridors in the northern part of the Los Angeles basin (Fig. 1). Wind speeds can also be very large in San Diego county, where the terrain gaps appear less prominent but also terrain heights are generally lower. We will see that in this part of Southern California, the flow across the topography shares many characteristics of classic downslope windstorms.

Downslope windstorms are a type of large amplitude mountain wave that can produce strong, often gusty winds on the lee side of a mountain barrier. Subsidence of air can cause very low relative humidities near the surface, particularly if the air mass starts with low absolute humidity. The necessary ingredients for downslope windstorms are a sufficiently large mountain barrier, as well as strong cross-barrier winds and a stable atmosphere, both near the mountaintop level (Chow et al. 2012). Downslope windstorms are observed in many areas of the world, and carry such names as the Bora, Chinook, Foehn, Zonda and Taku winds (Schamp 1964).

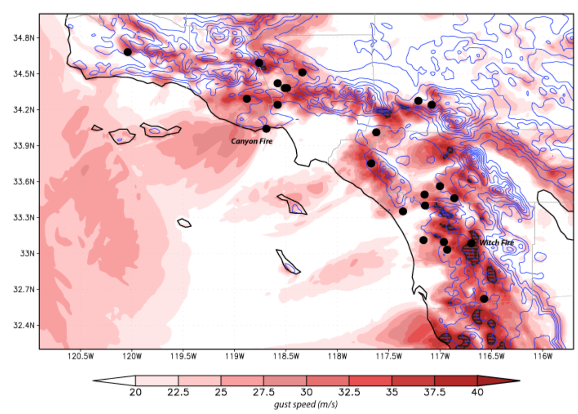

Fig. 1. Event maximum estimated wind gusts (colored) for the October 2007 Santa Ana wind event from a 2 km WRF-ARW simulation, illustrating wind corridors and shadows in Southern California. Values exceeding 40 m s^{-1} (90 mph) are hatched. Topography is shown in blue (300m contours). Black dots denote locations of fire ignition sites. Witch and Canyon fire sites are labeled.

In complex terrain, the wind can vary greatly over small distances and gustiness is common in downslope windstorms, which may be caused by subrotors embedded in the flow (Doyle and Durran 2007). Wind forecasts in this region are extremely important, since the gusty winds can knock down trees and power lines, starting and spreading fires. As an example, on 21 October 2007, the Witch Creek fire was sparked by wind-whipped power lines located about 20 m above ground level (AGL), and was driven by an especially strong Santa Ana wind event to become one of the largest fires in California history. This was but one of more than 25 fires that started during this event, all initiated in the regions characteristic wind corridors (Fig. 1).

There is great need to know, in advance, when the electrical grid is in danger, to reduce the risk of fire to this very fire-prone area. The purpose of this study is to understand how predictable the winds are in the San Diego area region and how skillfully a regional-scale weather prediction model can forecast the winds and especially the gusts that they even cannot resolve. The Weather Research and Forecasting (WRF) models Advanced Research WRF (ARW) core is selected for this exercise. Model validation and calibration will be carried out using a newly installed surface observing network of perhaps unprecedented density.

2. Available surface observations

Observations are crucial for vetting a numerical model, but there are several significant challenges involved. The surface wind observation station network has historically been relatively sparse and few stations have very long record lengths. Each network tends to measure the wind differently, with respect to sensor height and sampling, averaging and reporting intervals. Unfortunately, numerous stations have anemometers that are shielded by buildings and/or trees, or simply were not installed in the areas of greatest wind and/or hazard. Furthermore, above ground wind information is in even shorter supply.

In the last few years, the San Diego Gas and Electric (SDGE) company has deployed over 140 stations across San Diego county, purposefully placed in wind-prone areas (Fig. 2). These stations were designed to follow the RAWS (Remote Automated Weather Station) standard with respect to anemometer height (6.1 m or 20 ft AGL) and averaging interval for the sustained wind (10 min). Every 10 min, SDGE stations report sustained winds as well as maximum gusts based on 3-sec samples; this contrasts with the RAWS networks hourly reporting interval. The SDGE network may be the densest surface wind observations on the planet at this time, and captured a moderately strong Santa Ana wind event that occurred in middle of February 2013.

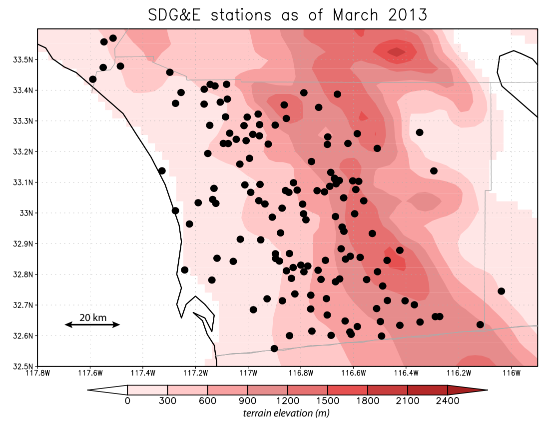

Fig. 2. SDGE surface station locations (black dots), with underlying topography shaded.

3. The 14-16 February 2013 event

In 2007, very high winds rushed through San Diego county, starting and spreading the infamous Witch Fire. At the time, however, few well-positioned and exposed stations existed, limiting our ability to calibrate and validate the model. Our strategy is to examine more recent Santa Ana events captured in the SDGE network. At this writing, these events have been considerably weaker than the October 2007 windstorm, but may provide important insights into the optimal model configuration with respect to model physics and resolution that are applicable to more intense events. Even though the current SDGE mesonet only provides us with information from a few meters above the ground, its high station density such as this will help us understand the spatial and temporal variation of the winds across this region, and can test the accuracy of the model simulations.

Although likely only moderate in overall strength as a Santa Ana event, some very impressive winds and gusts were recorded in the SDGE network during the mid-February event. For example, at 1830 UTC (1030 AM PST) on 15 February 2013, SDGE station Sill Hill (SIL) recorded a 41 m s^{-1} (91 mph) wind gust (Fig. 3), at a time when no other stations in this region recorded a wind gust greater than 26 m s^{-1} (57 mph). Indeed, the winds were 50% weaker at Boulder Creek (BOC), the SDGE station just 1.6 km to the south.

It would be easy to dismiss such a high wind observation. The wind record at that station (Fig. 4) shows, however, that the 91 mph gust was not an isolated occurrence. Over a 2-hour period, the SIL gust averaged 75 mph (34 m s^{-1}) and was frequently in the 80 mph (36 m s^{-1}) range before the 91 mph observation was recorded. (Note how similar the sustained wind at SIL is to the wind

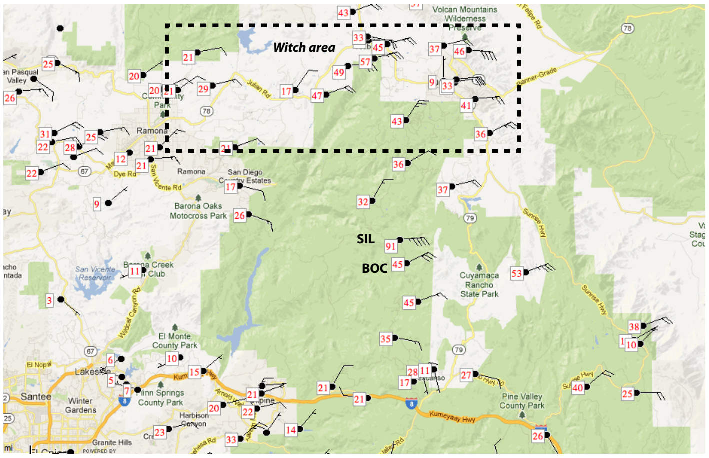

FIG. 3. Surface wind gusts (red numbers) and sustained winds (flags), both mph, at 1830 UTC (1030 AM PST) on 15 Feburary 2013, superposed on topography for the area. Distance between station SIL and BOC is 1.63 km (1 mile). Source: MesoWest and Google Maps.

gusts from BOC.) Furthermore, two SDGE meteorologists, Brian DAgostino and Steven Vanderburg, were at the site an hour before the fastest winds were recorded, and measured winds around 73 mph (33 m s^{-1}) at eye level with hand-held anemometers. A close inspection at the topographic map in the vicinity of SIL and BOC (not shown) indicates that SIL is sited on a small local ridge while BOC is in a local terrain crease, very small-scale factors that may be relevant to the wind speeds and exposures. This comparison helps illustrate the challenge that is faced in simulating and validating the winds across this area, as these very subtle terrain features would require extremely high resolution to capture.

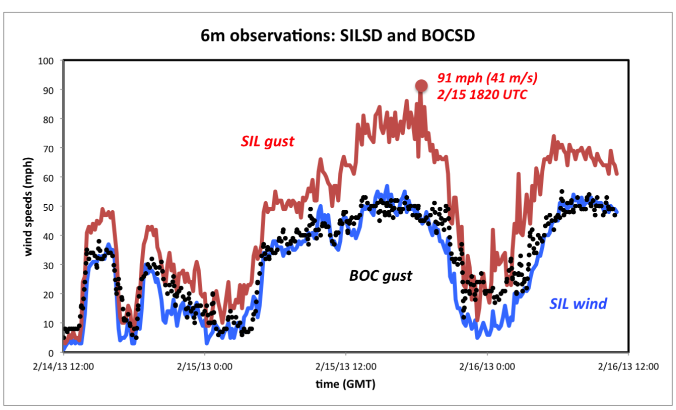

FIG. 4. Time series of observed winds (mph) at SIL and BOC over 2 days. Red and blue lines depict SIL gust and sustained wind, respectively; black dots denote BOC gust.

We now shift focus to the Witch Creek area, where there are many more SDGE stations available (Fig. 3). Station West Santa Ysabel (WSY) is located on the west-facing slope of the mountain, about 9-10 km down from the ridge (see Fig. 5a). Wind gusts observed there over a two-day period (Fig. 5b) reveal a Santa Ana episode consisting of two pulses separated by a protracted lull. The first phase peaked at 26 m s^{-1} (58 mph) at 1800 UTC (10 AM PST) on 15 Feb. After declining to as slow as 3 m s^{-1} (7 mph) during the afternoon, the gusts achieved similar strength by midnight local time before finally slowing as the event wound down.

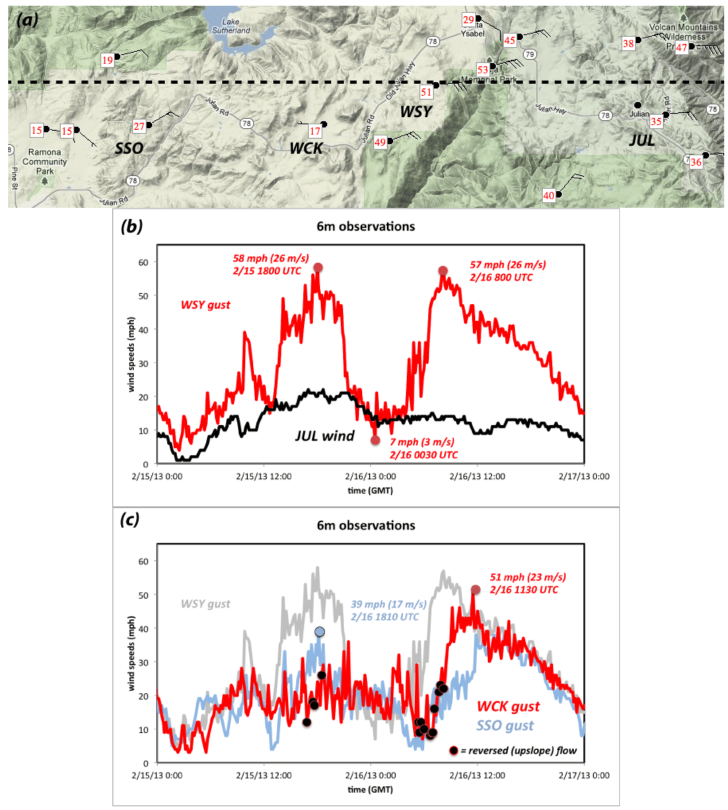

FIG. 5. (a) As in Fig. 3, but for surface wind (mph) observations at 1740 UTC (940 AM PST) on 15 February 2013 (source MesoWest), and time series of observations of (b) WSY gusts (red) and JUL sustained winds, and (c) WSY (black), WCK (red), and SSO (blue) gusts, over a period of 2 days. On (c), black dots indicate winds directed upslope at WCK.

In contrast, the sustained winds recorded at SDGE station Julian (JUL), which is near the top of the mountain ridge, reveal little in the way of temporal trend, apart from a long, slow decline through the period depicted (Fig. 5b). The winds also behaved very differently at Witch

Creek (WCK) station (Fig. 5c), which is less than 5 km downslope from WSY. During the first peak, WCKs winds remained much weaker than WSYs. Occasionally, the wind direction at WCK reversed to upslope (at times indicated by the black dots), suggesting a rotor or hydraulic jump may have formed there. During the lull between the two peaks, WSY and WCKs winds were comparably weak. WCK finally recorded strong winds during the second peak, but the winds lagged about 3 hours after WSY. While the winds were rising farther upslope, more wind reversals were observed at Witch Creek station.

Station Sunset Oaks (SSO) is 7 km farther downslope from WCK. Note that, during the first peak, its gusts were weaker than WSYs, but peaked at about the same time and were generally stronger than at WCK (Fig. 5c). The lull lasted longer at this station, and reached its second peak after the gusts at both WSY and WCK had started to decline. Taken together, these stations suggest a two-part Santa Ana event in which winds were largely in phase early in the event, apart from a suspected jump at WCK, and had a second part consisting of a marked downslope progression as the overall winds waned.

4. Vertical structure of the downslope flow

Although it provides no information above 6 m AGL, the dense SDGE surface observation network enables us to evaluate the realism of the model simulations of the terrain-amplified winds. This is important, as we have determined from hundreds of WRF simulations of this event alone that important characteristics of the downsloping flow are quite sensitive to resolution, landuse characteristics, model physics, and even random noise. Based on a systematic validation of model vs. observed winds, which will be explored in the next section, the physics ensemble member that appears to best represent the surface observations with respect to magnitude and temporal and spatial variation employed the Pleim-Xiu (PX) land surface model, ACM2 planetary boundary layer, and RRTMG radiation schemes. A simulation using this configuration in WRF version 3.5 and was initialized with North American Mesoscale (NAM) model forecasts at 1200 UTC 14 February 2013 (to represent an operational environment) will be examined in this section. A five-domain telescoping grid arrangement, with a 667 m nest that extended about 80 km west-east by 70 km north-south and covered roughly 70% of the SDGE network, is employed. The landuse database used was derived from MODIS observations.

Figure 6 presents the west-east vertical cross-sections across WSY (see Fig. 5a), with SSO, WCK, and JUL marked but being slightly out of the vertical plane depicted. At 0800 UTC 15 Feb 2013 (Fig. 6a), the downslope windstorm had started, but the winds near the ground at WSY and stations farther downslope had not yet begun to rise. Recall that by 1740 UTC, winds recorded at WSY and SSO had reached their first-phase peaks, but WCKs gusts remained weaker (Fig. 5c). Note the model simulation has developed a jump-like feature almost directly above WCK at this time (Fig. 6b), rendering relatively weak (and even occasionally reversed) winds there and stronger winds at WSY and SSO, consistent with the observations. Note also that, as expected, the wind speeds had not strengthened very much at JUL, which is located at the top of the ridge and at the very edge of the terrain amplification.

Five hours later, there was a brief period (around 2130 UTC) during which the winds at WCK were actually stronger than at the other stations (Fig. 5c). The winds at WSY and SSO were entering the lull period around that time, while the gusts at WCK had finally reached their first-phase peak of 36 mph (16 m s^{-1}). While the timing is not perfect, a similar phenomenon occurred in the model simulation. During this interval, the jump-like feature retreated upslope, passing over WCK (Fig. 6c).

As the jump retreated farther upslope, it also weakened and appeared to become more elevated (Fig. 6d). The model shows the lull period was one in which strong near-surface winds still existed, but became concentrated close to the ridge and in an area where there were no stations. The retreat occurred during the afternoon hours, and it is likely the shift in the character of the downsloping flow was responding to environmental changes on the upwind side. This is a subject of continuing research.

The second phase of the Santa Ana event ensued as the reintensifying flow began progressing downslope again after 0500 UTC (Figs. 5, 6e). Note another, smaller amplitude jump formed in the vicinity of WCK, again consistent with the observations. By midnight, however, that feature had disappeared and the downsloping flow became “flatter” and, eventually, shallower as the Santa Ana event eventually wound down (Figs. 6f-h). The observations indicated a westward progression in the peak near-surface wind speeds (Fig. 5c) occurred, and the model has largely captured this behavior.

5. Sensitivity to model physics and random perturbations

The physics sensitivity experiment in this section was conducted with WRF version 3.4.1, also using five domains telescoping to 667 m grid spacing but with the innermost nest focused more tightly on 25 stations in the Witch Creek vicinity. These simulations were also initialized with the aforementioned NAM model forecasts but utilized the USGS landuse database. Creating a physics ensemble involves an exhaustive examination of available model physical parameterizations, such as the land surface schemes, planetary boundary layer schemes, radiation schemes etc. In all, almost one hundred

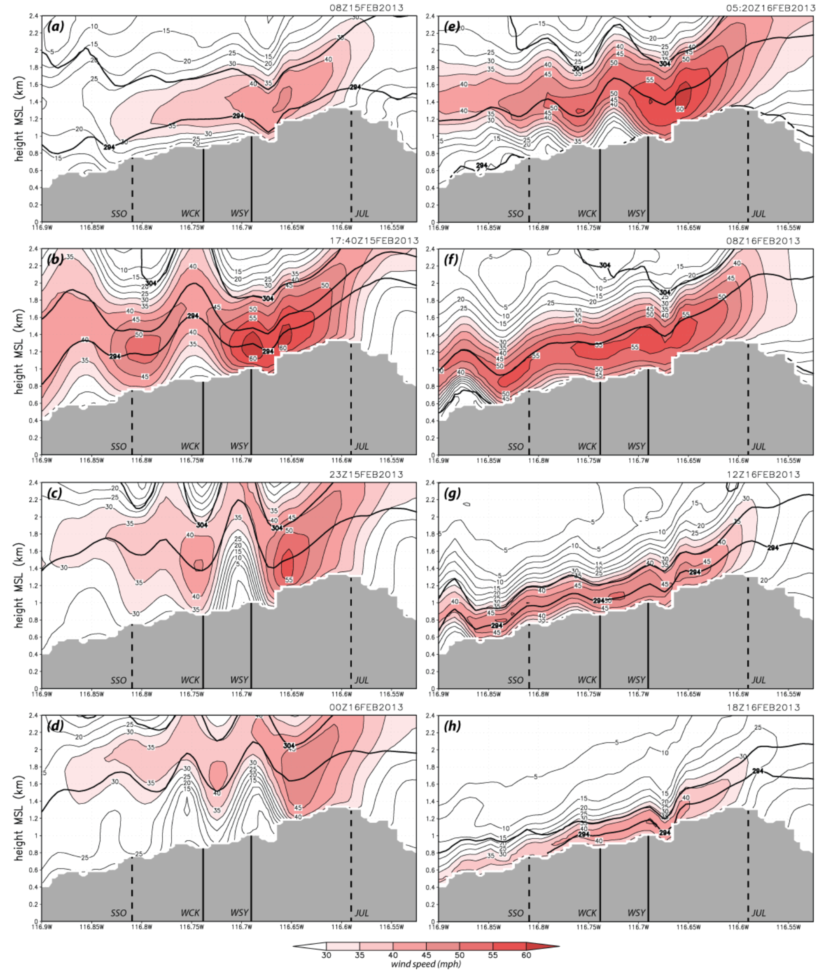

Fig. 6. Vertical cross-section of horizontal wind speed (5 mph interval thin contours), taken west-east across WSY with underlying topography shaded (see Fig. 5a). Red shaded field indicates wind speed. Thick contours denote isentropes (5K interval). Approximate locations of JUL, WSY, WCK and SSO are marked. WCK, SSO and JUL are a bit out of the vertical plane depicted.

combinations of model physics were examined.

As Fig. 7 reveals, not all model configurations are created equal. Shown is mean absolute error (MAE) of wind speed, relative to hourly observations from the SDGE network, averaged over the 54 h simulation period. The average event MAE spans 2.0-4.3 m s^{-1} (about 5-10 mph), with simulated wind speeds invariably overpredicted (not shown). Part of this is because the observed winds, recorded at 6 m (20 ft.), are being compared to the models 10 m flow speeds, which are computed diagnostically from the models lowest sigma level (about 26 m AGL) using the logarithmic wind relationship. Even correcting for the height difference does not completely mitigate the positive forecast bias, however (not shown).

The simulations are clearly sensitive to model physics, especially the land surface (LSM) scheme. Overall, the PX LSM was involved in the majority of the most accurate wind reconstructions when averaged over the 95 SDGE stations in the 667 m nest, with the Noah and MYJ schemes common among the poorest performers. It is perhaps not surprising that different model physics produces different wind speeds near the ground. Our analysis, however, suggests the most important aspect of the LSM was in how it handled the surface roughness (z_0). In the WRF model, the roughness for a particular location depends on the landuse category and database origin (such as USGS or MODIS). The PX scheme increases z_0 for many landuse categories, especially those most common on the west-facing slopes in San Diego county. We have found that altering other LSMs to increase the roughness of

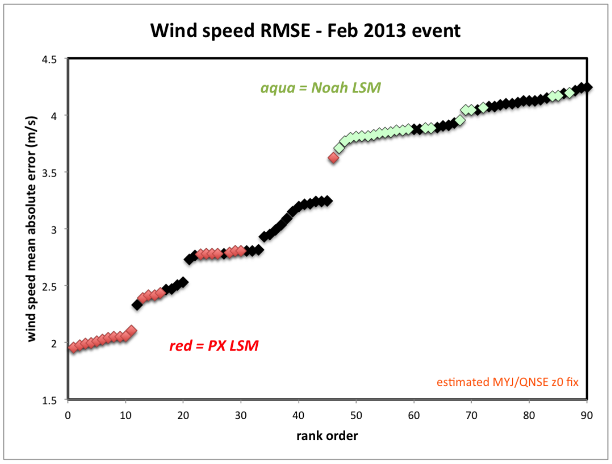

FIG. 7. Physics ensemble sustained wind speed mean absolute error (m s^{-1}), validated against SDGE network, in rank order. Red and aqua colors indicate PX and Noah LSM members, respectively. For members using the MYJ scheme, a standard but cosmetic recalculation of the near-surface winds was overridden.

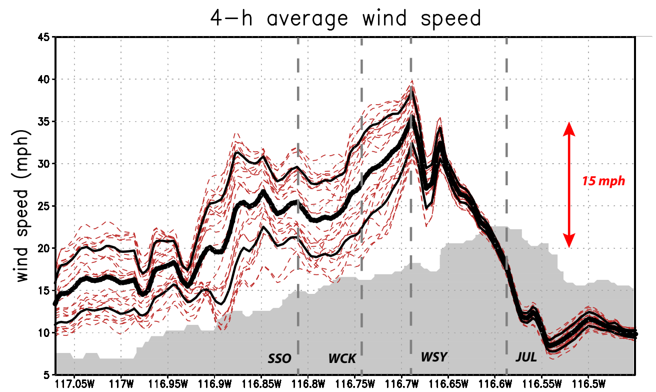

FIG. 8. Physics ensemble 4-hour average winds (mph) adjusted to SDGE anemometer height and centered on the WSY gust's first peak time (1800 UTC 15 February). Black lines are the ensemble mean, and ±1 standard deviations. Also shown is the underlying terrain (shaded).

those categories improved their MAE and bias scores (not shown).

It is intuitive that increasing the surface roughness should slow down the winds. However, it also changes the nature of the downsloping flow, at least in this case. One of the remarkable characteristics of the 14-16 February event, especially its first phase, was the development of the jump-like feature and wind reversal above WCK. It has emerged that only the LSMs that employed relatively larger z_0 values were able to capture this feature, which the observations indicate was prominent and persistent. The smoother the terrains lee side, the faster and more uniform the flow that developed there was, preventing the WCK jump from forming and resulting in faster than observed winds farther down the slope.

Figure 8 presents four-hour average winds from about 40 of the physics ensemble members, centered on the time of WSYs first peak and WCKs first wind reversals. The winds have been adjusted to SDGE anemometer height using the logarithmic wind profile, which is a function of z_0, stability, and the diagnosed 10 m wind. Note the variation among the ensemble members was quite small upwind of, and past, the ridge, until the flow passed the narrow canyon just upslope from WSY. From that point downslope, the variation has become quite substantial, in the very region where the need for skillful forecasts is crucial. As suggested by the figure, few of the physics ensemble members have reconstructed weak winds for the Witch Creek area, although a local minimum is indicated between WCK and SSO.

We have found that wind speed MAEs and positive biases were reduced by adopting the MODIS landuse database instead of the WRF default USGS dataset. Although these databases categorize the landscape somewhat differently, the MODIS version narrows a zone of high roughness ($z_0 \approx 0.5$ m) near the ridge but also generally increases the drag across the west-facing slope, including placing a locally rough area ($z_0 \approx 0.24$ m) just upslope from WCK (not shown). In contrast, the USGS surface roughness during winter in this area is only 0.01 m, with no variation at all in the vicinity of WCK. The PX LSM increases these MODIS values further almost everywhere, with WCK area roughnesses being as large as 0.75 m, 7500% larger than the USGS specification. It is surmised that increasing the surface drag played a major role in the ability of the PX ensemble members to create the Witch Creek jump.

That being said, it has also emerged that the wind reconstructions for this case possessed a tremendous amount of inherent uncertainty as well. This was demonstrated by introducing random noise into the simulations using the stochastic kinetic energy backscatter scheme (SKEBS) in WRF (Shutts 2005). This scheme inserts its perturbations where and when turbulence is diagnosed, which is substantial on the downslope side, especially at and below WSY. We examined two perturbation ensembles, using WRF version 3.5, the large 667 m resolution domain, and the MODIS database. The first ensemble employed the popular Noah/YSU physics combination, while the second adopted the PX/ACM2 physics combination, which was judged as the best one among the physics ensemble.

Figure 9 shows the 4-hour averaged anemometer-level winds around the occurrence of the first wind peak at WSY for the Noah/YSU random perturbation ensemble, for comparison with Fig. 8. Note the structure of the winds across the upper part of the terrain is now different; this reflects the adoption of the MODIS roughnesses. Again, the spread increased at and past WSY, and now uncertainty was largest near WCK, with winds spanning 7-38 mph. Vertical cross-sections (not shown) reveal that some of the members still did not produce jumps over WCK, while many others did, although obviously with a variety of positions relative to the station (Fig. 9).

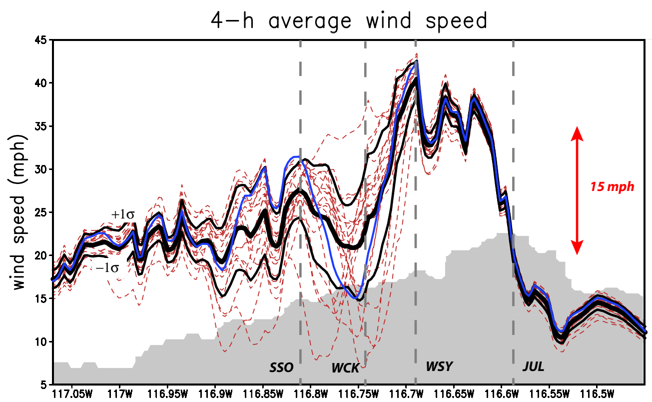

FIG. 9. As in Fig. 8, but for the Noah/YSU MODIS-based perturbation ensemble.

The magnitude of the perturbation ensembles variability is remarkable, as it exceeds that seen in the physics ensemble. It is speculated that the generally rougher surface assumed by the MODIS database is important to enhancing this sensitivity. Increasing the roughness further, however, appears to start dampening the sensitivity, which appears sensible. The PX/ACM2 physics combination (Fig. 10) produced slower and less variable winds overall, with a greater likelihood of positioning the jump over WCK. Again, revising z_0 values in Noah/YSU simulations tended to make the flow patterns and speeds more like those produced by PX/ACM2 (not shown).

6. Gust estimation

Short period (3-sec) gusts cause severe damage, yet mesoscale models are not able to directly simulate them. The winds generated by the model should be compared to sustained winds, as even with the small time steps associated with the high-resolution simulations fail to capture high-frequency variability associated with turbulence. A variety of techniques, ranging from simple and sophisticated, can be employed to diagnose the gusts from the model (e.g., Fovell 2012), one of these involving

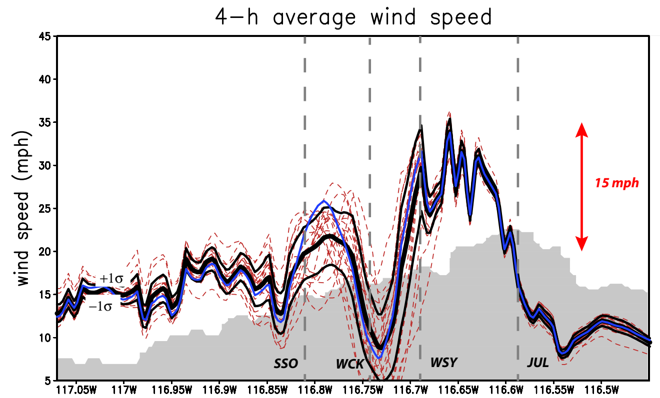

FIG. 10. As in Fig. 8, but for the PX/ACM2 MODIS-based perturbation ensemble.

the application of a gust factor (GF) to the models diagnosed winds (after sensor height adjustment). This is not a particularly rewarding strategy when a gridded output field is needed, as the GF will vary from place to place, reflecting locational characteristics, and is also generally dependent on the magnitude of the sustained wind.

The literature suggests that a typical GF for a well-exposed site in flat terrain is about 1.4-1.5, although this depends on atmospheric stability, the sustained wind speed, surface roughness, observation height, and averaging interval for the sustained wind as well as the sampling interval for the gust (e.g., Durst 1960; Wieringa 1973; Schroeder et al. 2002). As an example, Fig. 11 displays the distribution of GF with sustained wind for SDGE station SIL calculated from 38600 observations recorded during 2012 and 2013. We see that as the 10-min average wind gets stronger, the GFs magnitude and range both decrease, to roughly 1.25 for the very fastest observations. This hints the commonly used typical GF value of 1.4 may be not generally appropriate. Certainly, some polynomial function could be fitted to these data, providing some insight into the gust strengths that might be expected given a particular model-predicted sustained wind. However, the 91 mph gust mentioned in Sec. 3 that occurred with the sustained wind was only 45 mph (20 m s^{-1}), so such a function would have seriously underpredicted that very fast wind sample.

There are a variety of techniques for relating observed near-surface gusts to some function of the resolved flow speeds in the boundary layer (e.g., Brasseur 2001). Thus far, we have found a fair amount of success using the simulations wind speed at the first model level alone (approximately 26 m AGL) to represent the gust, at least when the PX and ACM2 schemes are used with their

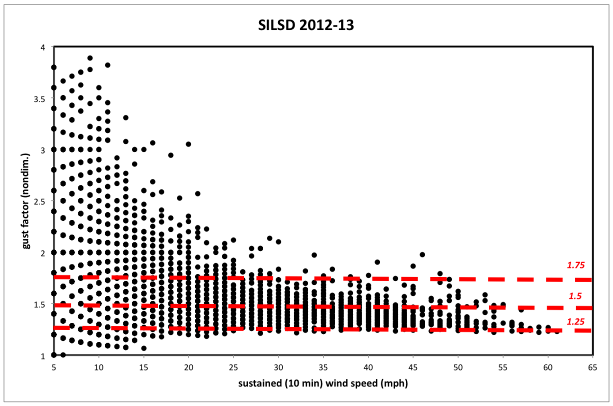

FIG. 11. Gust factors (nondimensional) calculated from 38600 observations for the SDGE station at Sill Hill (SIL) for observations collected during parts of 2012 and 2013, plotted against the sustained 10 minute wind speed (mph).

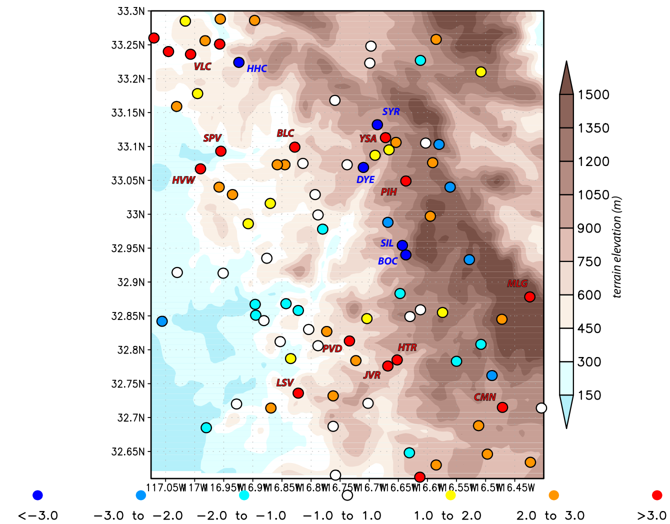

FIG. 12. Average event gust bias (m s^{-1}) map for the 14-16 February 2013 event for the gust proxy using the first model level simulated wind. Warm colors denote stations with overpredicted gusts, while cold colors indicate underpredicted locations, with underlying topography shaded.

revised MODIS roughnesses. Our validations are limited to 95 SDGE stations in the 667 m domain, comparing the 26 m simulated wind on the hour to the fastest 6 m wind gust reported during the previous hour.

Figure 12 shows the average event bias map for this wind gust proxy over the February 2013 Santa Ana event. Clearly, some stations are systematically over- or underpredicted, reflecting terrain variations that are subgrid, even at this relatively high resolution. Overforecasted station YSA is sited very close to a sharply rising hill, and thus probably in a very localized wind shadow. Station SYR, just 2.5 km away, is sited a little farther away from this same north-south terrain feature, and its winds were substantially underforecasted. PIH resides downslope of perhaps the thickest canopy of trees remaining in the San Diego backcountry, bringing roughness values and logarithmic wind profile applicability into question, while MLG, near the ridge, is known to have been improperly sited immediately behind trees. The model gusts at SIL were consistently stronger than the simulated winds anywhere in the boundary layer; both SIL and DYE have small-scale terrain features that may be helping locally amplify the flow. As a consequence of this, multiple techniques for gust forecasts are being considered. There is no "one size fits all" method, indicating a demand for an ensemble approach for gust predictions.

A major goal of this work is to produce a wind map of San Diego county, to determine how fast the wind has been at various places using model simulations of the past, calibrated against modern observations. A preliminary example that was developed from 41 high wind past events is shown in Fig. 13. Ultimately, to determine the wind threat, we also need to investigate the sensitivity of the Santa Ana winds to potential, near-term climate change. This represents future work.

7. Summary

We have closely examined the 14-16 February 2013 Santa Ana event, which was characterized by a moderately intense downslope windstorm in the Laguna mountains of San Diego county. The unprecedented, dense SDGE mesonet is enabling enhanced insights into the terrain-amplified wind events. We have shown that the windstorm flow speeds and patterns were sensitive to model configuration, especially the land surface schemes and landuse database, which determine the surface roughness that modulates the strength of the downslope flow at the surface. Sensitivity to random noise was also substantial. The models 26 m sustained wind showed promise for forecasting gusts recorded at anemometer-level, at least for certain model configurations and during downslope windstorms. In addition to implementing an operational gust forecasting capability, we also intend to produce a wind map for San Diego, providing guidance on maximum potential winds and recurrence intervals.

Acknowledgments.

This research was sponsored by San Diego Gas and Electric company.

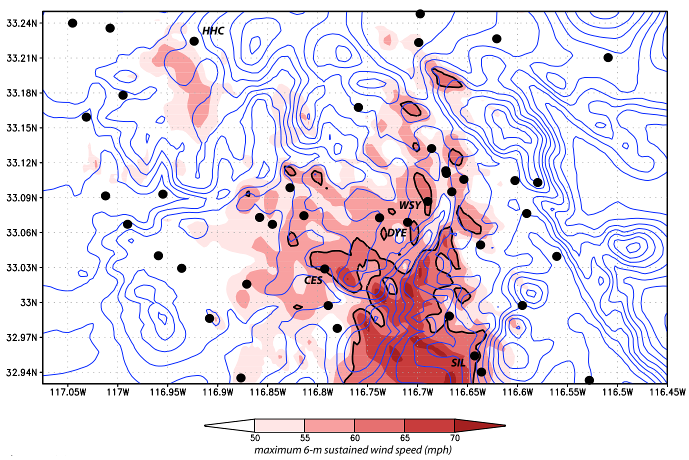

FIG. 13. Preliminary maximum wind map over the Witch area, representing a composite of high wind events over a 60-year period. Maximum 6-m wind speeds (mph) are shaded, with superposed topography contoured. Some SDGE station locations are indicated.

REFERENCES

Brasseur, G., 2001: Development and application of a physical approach to estimating wind gusts. *MWR*, **129**, 5–25.

Chang, C.-H. and F. P. Schoenberg, 2011: Testing separability in marked multidimensional point processes with covariates. *Ann. Inst. Stat. Math.*, **63**, 1103–1122.

Chow, F. K., S. F. D. Wekker, and B. J. Snyder, 2012: *Mountain Weather Research and Forecasting: Recent Progress and Current Challenges*. Springer, 750 pp.

Doyle, J. D. and D. R. Durran, 2007: Rotor and subrotor dynamics in the lee of three-dimensional terrain. *J. Atmos. Sci.*, **64**, 4202–4221.

Durst, C. S., 1960: Wind speeds over short periods of time. *Meteor. Mag.*, **89**, 181–186.

Fovell, R. G., 2012: Downslope windstorms of San Diego county: Sensitivity to resolution and model physics. *13th WRF Users Workshop*, Boulder, CO, Nat. Center for Atmos. Res.

Glickman, T., 2000: *Glossary of Meteorology*. Amer. Meteor. Soc., 855 pp.

Raphael, M. N., 2003: The Santa Ana Winds of California. *Earth Interact.*, **7**, 1–13.

Schamp, H., 1964: *Die Winde der Erde und ihre Namen*. Franz Steiner Verlag, 94 pp.

Schroeder, J. L., M. R. Conder, and J. R. Howard, 2002: Additional Insights into Hurricane Gust Factors. *25th Conf. on Hurricanes and Tropical Meteorology*, San Diego, CA, Amer. Meteor. Soc., 39–40.

Shutts, G., 2005: A kinetic energy backscatter algorithm for use in ensemble prediction systems. *Quart. J. Roy. Meteor. Soc.*, **131**, 3079–3102.

Wieringa, J., 1973: Gust factors over open water and built-up country. *Boundary Layer Meteor.*, **3**, 424–441.